CWE-8
June 7-11, 2026
London, ON, Canada

Numerical study on the aerodynamic properties of rectangular prism with side ratio of two rotating at a constant speed

K. Noguchi [a], R. Horie [b], H. Matsumiya [c], R. Katayama [d], T. Yagi [e]

[a]*Kyoto University, Kyoto, Japan, noguchi.kyohei.7z@kyoto-u.ac.jp*
[b]*Kyoto University, Kyoto, Japan, horie.risa.77h@st.kyoto-u.ac.jp*
[c]*Kyoto University, Kyoto, Japan, matsumiya.hisato.4y@kyoto-u.ac.jp*
[d]*Kyoto University, Kyoto, Japan, katayama.riki.g10@kyoto-u.jp*
[e]*Kyoto University, Kyoto, Japan, yagi.tomomi.7a@kyoto-u.ac.jp*

SUMMARY

When calculating two-variable aerodynamic coefficients consisting of torsional displacement and nondimensional torsional velocity based on the aerodynamic force acting on a rectangular prism rotating at a constant speed, radial stripes are observed in the contour diagram. However, whether this distribution truly corresponds to aerodynamic phenomena is not sufficiently verified. In this study, a two-variable lift coefficient was calculated using a two-dimensional unsteady RANS analysis. It was determined that the stripes existed in both the experimental and numerical contours, indicating that the stripes corresponded to an aerodynamic phenomenon. Furthermore, by investigating the frequency characteristics of the unsteady lift, the striped pattern in the contour diagram was found to originate from vortex shedding. When the nondimensional torsional velocity was small, vortices were shed at a frequency corresponding to the stationary condition at the instantaneous torsional displacement. However, as the torsional velocity increased, vortex shedding became independent of the torsional velocity.

Keywords: *constant-speed rotation, two-variable aerodynamic coefficients, torsional velocity term, RANS*

1. INTRODUCTION

In the wind-resistant design of structures, including long-span bridges, the occurrence of aerodynamic self-induced vibrations is critical, and therefore numerous studies have focused on the small-amplitude regions near the onset wind speed. However, large-amplitude responses at wind speeds higher than the onset wind speed have not been sufficiently investigated, leaving several issues unresolved. Although the quasi-steady aerodynamic force is a candidate model for evaluating large-amplitude responses, they do not include a torsion velocity term, which makes it difficult to analytically determine large-amplitude torsional responses. Matsumiya et al. (2018) demonstrated that the large-amplitude response of four-bundled conductors can be appropriately represented by formulating two-variable aerodynamic coefficients based on torsional displacement and velocity. Matsumiya et al. (2025) successfully determined two-variable aerodynamic coefficients for arbitrary combinations of torsional displacement and velocity by measuring the aerodynamic force acting on a rectangular prism rotating at various constant speeds. However, when the two-variable aerodynamic coefficients obtained from wind tunnel tests are plotted as a contour diagram for torsional displacement and velocity, radial stripes appear. It remains unclear whether these stripes correspond to aerodynamic phenomena or are merely pattern dependent on the measurement conditions. This study aims to clarify the aerodynamic properties during constant-speed rotation by calculating the aerodynamic force acting on a rotating rectangular prism using Reynolds-averaged Navier–Stokes (RANS) simulations to obtain the two-variable aerodynamic coefficients.

2. NUMERICAL METHODS

Two-dimensional (2-D) unsteady RANS with the *k–ω* SST model was used for flow-field analysis. OpenFOAM (v2206) was employed to analyze a rectangular prism, with a side ratio of *B/D* = 2 (*D*: height, *B*: width), rotating at a constant speed. Figure 1 shows the computational domain, which was created as an O-type structured grid (460 grids in the circumferential direction and 200 grids in the radial direction) with a radius of 70*B*. The height of the grids adjacent to the wall was *B*/2,000. The constant-speed rotation of the rectangular prism was simulated by rotating the entire computational domain as a rigid body. The "freestream" boundary condition was applied to the far-field boundary. This condition automatically determines the inflow (fixed velocity and zero-pressure gradient) and outflow (zero-velocity gradient and zero pressure) based on the flux through the internal grid, allowing for a flexible boundary condition setting even when the computational domain itself rotates. The rotational speed was set to 43 different values within a range of $30 \leq TU/B = 2\pi U/\dot{\theta}B \leq 600$, where *T*: rotation period, *U*: inflow wind speed, and $\dot{\theta}$: rotational speed (torsional velocity or angular velocity). Pressure–velocity coupling was performed using the PIMPLE method. A second-order implicit scheme was used for time progression, second-order linear scheme with a TVD limiter (equipped as MUSCL in OpenFOAM) for the convection term, and second-order linear scheme for the diffusion term. For shapes where the separation point is fixed, such as bridge girders and rectangular prisms, the lower limit of the Reynolds number has been proposed to set to 10,000 (JSCE, 2023). Therefore, the Reynolds number defined with *D* was set to 10,000. The nondimensional time increment was set to $\Delta tU/B = 0.02$. The ensemble average of five rotations (equivalent to 10 wave periods owing to vertical symmetry) after flow-field stabilization was used for the subsequent discussions. This study addressed a two-variable lift coefficient, ${C_L}^*$, as in Eq. (1), derived from the unsteady lift, $Lift$ (defined on the wind axis, upward positive). We confirmed that similar results were obtained for unsteady aerodynamic moments. Due to space constraints, this has been omitted.

$$ {C_L}^*\left(\theta, b\dot{\theta}/U\right) = Lift\left(\theta, \dot{\theta}\right)/(0.5\rho U^2 Bl) \tag{1} $$

where θ: torsional displacement (head-up positive), ρ: air density, l: span length, and $b = B/2$.

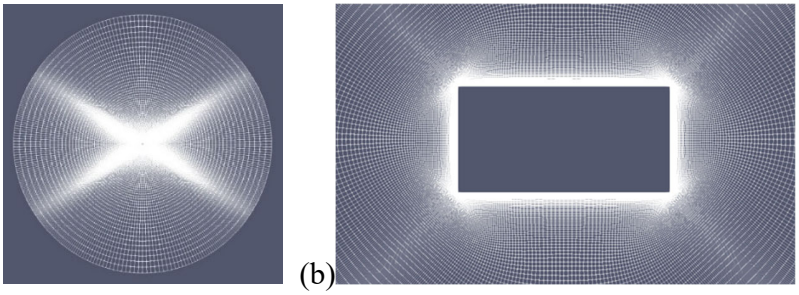

Figure 1: Computational domain. (a) Entire view and (b) enlarged view.

This study used a 2-D RANS to reduce the computational load and enable the evaluation of numerous torsional velocity cases. However, 2-D analysis of small-aspect-ratio rectangular prisms cannot adequately reproduce their aerodynamic properties (Tian et al., 2013). In this study, the time-averaged drag coefficient under the stationary condition was also overestimated within a certain range of angles of attack. Although this could potentially affect the results at specific moments during the rotation, the trend of the time-averaged aerodynamic coefficients associated

with the angle of attack was successfully reproduced. Therefore, the approach used in this study enabled a qualitative discussion relevant to the research objectives. Quantitative verification remains a future work.

3. RESULTS AND DISCUSSIONS

Figure 2 shows the experimental (Matsumiya et al., 2025) and numerical results for $C_L{}^*$. The horizontal axis represents the torsional displacement θ, and the vertical axis represents the nondimensional torsional velocity $b\dot{\theta}/U$. Notably, the motion trajectory during constant-speed rotation formed a straight horizontal line. The distributions of $C_L{}^*$ were similar for the experimental and numerical results, indicating that the numerical results were reasonable. Furthermore, radial stripes were visible in both cases, suggesting that this distribution originated from aerodynamic phenomena.

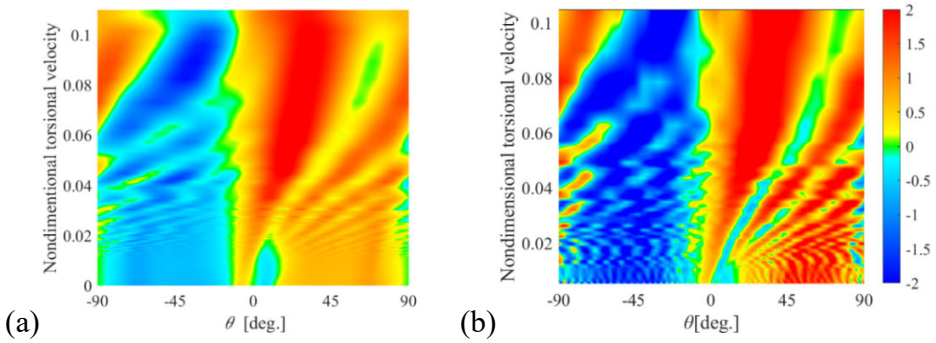

Figure 2: Two-variable lift coefficients. (a) Experimental and (b) numerical results.

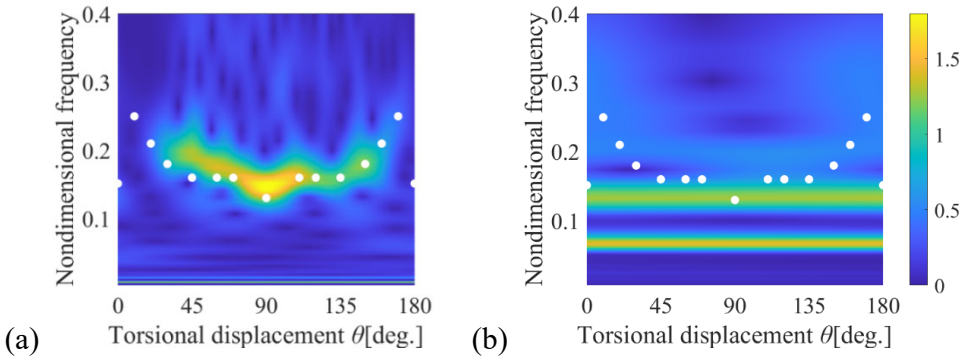

Figure 3: Dominant vortex shedding frequencies during constant-speed rotation. (a) $b\dot{\theta}/U = 0.0105$ and (b) 0.105.

A wavelet analysis was performed on the unsteady lift during rotation to examine the aerodynamic properties represented by these stripes. Examples for (a) when $b\dot{\theta}/U$ is small and (b) when $b\dot{\theta}/U$ is large are shown in Figure 3. The horizontal axis represents θ, and the vertical axis shows the nondimensional vortex shedding frequency fB/U. Two dominant frequencies appear in both cases. One appears linearly in the low-frequency range ((a) $fB/U = 0.0067$, (b) 0.067), matching the inverse of the time for half-rotation, suggesting that it originates from aerodynamic properties owing to rotation. The other appears in the approximate range of $0.1 < fB/U < 0.2$, but its characteristics differ depending on $b\dot{\theta}/U$. In Figure 2(a), where $b\dot{\theta}/U$ is small and rotation is slow,

fB/U depends on θ, matching the Strouhal number (white circles) obtained from the lift under the stationary conditions at each θ. Conversely, as $b\dot{\theta}/U$ increases, fB/U ceases to depend on θ, becoming a constant value in Figure 2(b). This frequency is nearly equal to the Strouhal number of $\theta = 0°$ or $90°$. Although the dependence on θ varies in $b\dot{\theta}/U$, fB/U is ~0.15 in all cases. Supposing that this value is applicable to arbitrary situations for simplicity, the torsional displacement during n events of vortex shedding θ_n (n: natural number) is calculated as in Eq. (2).

$$\theta_n[\mathrm{deg}] = \frac{n}{0.15} \times \frac{b\dot{\theta}}{U} \times \frac{180}{\pi} \leftrightarrow \frac{b\dot{\theta}}{U} = \frac{1}{n} \times \theta_n \times \frac{\pi}{180} \times 0.15 \tag{2}$$

This indicates that θ_n increases as $b\dot{\theta}/U$ increases. Furthermore, θ_n was found to correspond approximately to the width of the stripes in the contour plot, as shown in Figure 4. Thus, the radial stripes in the contour plot correspond to vortex shedding during rotation.

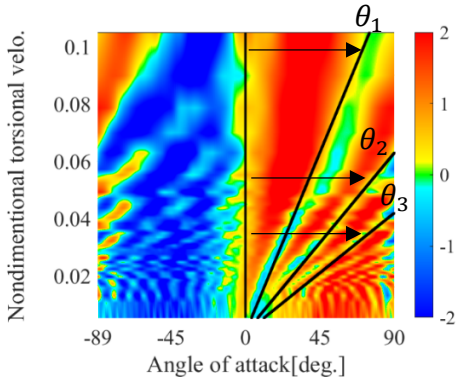

Figure 4: Two-variable lift coefficient obtained from RANS and displacement during vortex shedding.

4. CONCLUSIONS

Calculating the aerodynamic force acting on a rectangular prism rotating at a constant speed using 2-D unsteady RANS revealed that the radial stripes appearing in the contour plot of the two-variable aerodynamic coefficients originated from vortex shedding. When the nondimensional torsional velocity was small, vortices were shed at frequencies corresponding to the stationary condition at the instantaneous torsional displacement. However, as the torsional velocity increased, vortex shedding became independent of the torsional velocity.

ACKNOWLEDGEMENTS

The supercomputer of ACCMS, Kyoto University, was used for the flow analyses.

REFERENCES

JSCE (Japan Society of Civil Engineers), 2023. Guideline for application of computational fluid dynamics on wind-resistant design of bridges. Structural Engineering Series, 30. JSCE, Japan.

Matsumiya, H., Nishihara, T., Yagi, T., 2018. Aerodynamic modeling for large-amplitude galloping of four-bundled conductors. J. Fluids Struct. 82, 559-576. https://doi.org/10.1016/j.jfluidstructs.2018.08.003

Matsumiya, H., Katayama, R., Taruishi, S., Noguchi, K., Yagi, T., 2025. Time-history response analysis of rectangular cylinders using a new unsteady aerodynamic force model considering aerodynamic nonlinearity, in: Proceedings of the 10th Asia-Pacific Conference on Wind Engineering (APCWE10), #1-25.

Tian, X., Ong, M.C., Yang, J., Myrhaug, D., 2013. Unsteady RANS simulations of flow around rectangular cylinders with different aspect ratios. J. Ocean Eng. 58, 208-216. https://doi.org/10.1016/j.oceaneng.2012.10.013